Validation of a Two-Phase CFD Model for Predicting Tank Self-Pressurization in the Ground-Based K-Site Experiment

Olga Kartuzova[1] and Mohammad Kassemi[2]
National Center for Space Exploration Research (NCSER), Case Western Reserve University and NASA Glenn Research Center, Cleveland, OH 44135, USA
Daniel Hauser[3]
NASA Glenn Research Center, Cleveland, OH 44135, USA

A two-phase CFD model for self-pressurization of a cryogenic storage tank partially filled with liquid hydrogen is presented using the Volume-Of-Fluid approach for modeling two-phase flow, as well as interfacial heat, mass and momentum transfer between the liquid and vapor regions. The CFD model is validated against self-pressurization experiment performed using the K-site flightweight hydrogen storage tank at NASA Glenn Research Center[1]. Laminar and turbulent simulations are performed together with conjugate heat transfer analysis. Effects of turbulence, the value of accommodation coefficient used for predicting phase change rates, as well as tank wall geometry are presented and discussed. Predicted tank pressures, fluid and wall temperatures are compared with the experimental data at 49% fill level and two different heat loads for validating this CFD model.

I. Nomenclature

E	=	energy, J
F	=	force, N
g	=	gravitational acceleration, m/s^2
h	=	enthalpy, J/kg
k	=	thermal conductivity, W/m·K
n	=	normal vector
p, P	=	pressure, Pa
t	=	time, seconds
T	=	temperature, K
v	=	velocity, m/s

Greek

α	=	cell value of volume fraction
μ	=	Pa·s
ρ	=	density, kg/m^3
σ	=	surface tension, N/m

Subscripts

eff	=	effective
i	=	interface
q	=	phase

II. Introduction

Predicting rates of tank pressure increase when heat leaks into a cryogenic storage tank through insulation, structural support and tank penetrations is important for NASA's short and long duration missions. When heat is added to a cryogenic tank it causes an increase in liquid and vapor temperatures, evaporation of the liquid at the interface and an increase in tank pressure. This process is referred to as tank "self-pressurization". It is important to be able to accurately predict tank pressure and temperature increases during tank self-pressurization so passive and active processes can be designed to control tank pressure and preserve an integrity of the tank wall. A computational model has been developed and validated against tank self-pressurization experiments with a 4.89 m^3 liquid hydrogen storage tank, as reported by Hasan et al. in the 1991 paper[1]. In the experiments a tank (known as K-Site tank) filled with liquid hydrogen and its vapor was used. Test cases with 49% fill level and two different values of heat flux entering through the tank wall (2 W/m^2 and 3.5 W/m^2) were selected for model validation.

[1] Research Assistant Professor, Department of Mechanical & Aerospace Engineering.
[2] Research Professor, Department of Mechanical & Aerospace Engineering, AIAA Associate Fellow.
[3] Fluids Engineer, Fluid and Cryogenic Systems Branch.

A number of computational studies, as summarized by Lan et al.[2], both using nodal and Computational Fluid Dynamics (CFD) models were performed in an attempt to study tank self-pressurization under 1g and microgravity conditions. Kassemi et. al.[3] presented CFD model validations against both 1g and microgravity experiments conducted in small-scale tanks with simulant fluids, as well as a large-scale tank filled with cryogenic fluid. In their paper laminar CFD models showed good agreement with the experimental pressures and temperatures. However, turbulent model applied to simulating self-pressurization in a large-scale tank in 1g, where natural convection flow and heat transfer are turbulent, significantly under-predicted tank pressure rise. Kartuzova et al.[4] presented similar findings in their 2014 paper, where they modeled self-pressurization of a large-scale tank in 1g. They also showed that the turbulent model (k omega SST in this case) significantly under-predicted tank pressure and ullage temperatures during self-pressurization.

This paper investigates a different approach to turbulence modeling. Rather than using traditional Reynolds-Averaged Navier Stokes (RANS) turbulence models, which perform poorly when applied to cryogenic storage tank self-pressurization problems, a scale resolving Improved Delayed Detached Eddy Simulation (IDDES) model is applied. The results of this model are compared with the results of the RANS models, laminar model, and experimental data.

Details of the CFD model and validation results are presented in this paper. Predicted tank pressures, as well as fluid and tank wall temperatures are compared with experimental data. Effects of turbulence modeling, tank wall geometry and accommodation coefficient, used in phase change rate calculations are examined. Two different wall heat fluxes are considered.

III.Experimental setup

The flightweight tank considered in the experiment has a low mass-to-volume ratio and high-performance multi-layer thermal insulation, which is representative of spacecraft tanks. In the experiment the test tank is suspended by fiberglass composite struts in a vacuum chamber and enclosed in a cylindrical cryoshroud. The tank is made of 2219 aluminum and insulated with two blankets of multi-layer insulation each comprised of 17 layers of double aluminized Mylar separated by silk netting. It is approximately an ellipsoidal volume of revolution with a major to minor axis ratio of 1.2 a major diameter of 2.2 m and a volume of 4.89 m^3. The tank wall has a variable thickness with most of the wall being 2.08 mm thick, except for the bolted flange and lid at the top, lands for support lugs, and thickened equatorial region, as shown in Fig. 1a. Liquid fill level in the experiment is measured by a capacitance probe with accuracy of ± 1.9 cm, which is equivalent to ± 1.5% fill at the 50% fill level by volume. Liquid and vapor temperatures in the tank are measured by silicon diode transducers with accuracy of ± 0.3K. Mounted silicon diode transducers are used to measure external wall temperature distribution with accuracy of ± 0.6 K. A schematic of the tank with fluid and wall temperature probe locations used for comparison in this study is shown in Fig. 1b. Tank pressure is measured by pressure transducers located in the vent line with accuracy of ± 0.01 kPa.

In the experiment a boil off test was conducted first to condition the tank and insulation system and to determine the total heat leak rate into the tank. Boil-off testing and measured heat loads are discussed by Stochl and Knoll in their 1991 paper[5]. After static conditions were obtained in the boiloff test the tank was prepared for the self-pressurization tests. First tank vent valves were closed, and the tank was slowly drained to the level slightly above the desired fill level. Next the tank pressure was reduced to atmospheric pressure of 103 kPa by venting. After this the self-pressurization test began.

IV.Mathematical Model

A. Governing Equations

Fluid flow and heat transfer in the tank are described in terms of the continuity, Navier-Stokes and energy equations for both phases:

$$\frac{\partial \rho}{\partial t} + \nabla(\rho \mathbf{v}) = 0, \tag{1}$$

$$\frac{\partial}{\partial t}(\rho \mathbf{v}) + \nabla(\rho \mathbf{v}\mathbf{v}) = -\nabla p + \nabla\left[\mu_{eff}(\nabla \mathbf{v} + \nabla v^T)\right] + \rho \mathbf{g} + \mathbf{F}_{vol}, \tag{2}$$

$$\frac{\partial}{\partial t}(\rho E) + \nabla\left(\mathbf{v}(\rho E + p)\right) = \nabla\left(k_{eff}\nabla T\right) + S_h. \tag{3}$$

In the present study, the liquid phase is treated as incompressible. The liquid density is allowed to vary linearly with temperature in the body force term of the momentum equation according to the Boussinesq approximation. The

vapor is modeled as a compressible ideal gas. In this study, the movement of the interface is captured diffusely using the Volume-Of-Fluid (VOF) method, as promogulated by Hirt and Nichols[6]. Interfacial energy, momentum and mass balances are applied using source terms in the diffuse interfacial region.

B. VOF Model

In the VOF method, a volume fraction is defined in each cell such that the volume fractions of all the phases sum to unity. In the cell, the change in the interface can be tracked by solving a continuity equation for the volume fraction of the q^{th} phase:

$$\frac{1}{\rho_q}\left[\frac{\partial}{\partial t}(\alpha_q \rho_q) + \nabla \cdot (\alpha_q \rho_q \mathbf{v}_q) = S_{\alpha_q}\right], \tag{4}$$

where the volume fraction for the primary phase is determined from:

$$\sum_{q=1}^{n} \alpha_q = 1. \tag{5}$$

In the VOF method, the field variables and properties are defined in terms of the volume fraction, which for a general system can be written as:

$$\rho = \sum_{q=1}^{n} \alpha_q \rho_q, \qquad \mu_{eff} = \sum_{q=1}^{n} \alpha_q \mu_{eff_q}, \qquad k_{eff} = \sum_{q=1}^{n} \alpha_q k_{eff_q}. \tag{6}$$

In this fashion, the continuity, momentum and energy equations, as described by Eq. (1) – (3), can be solved throughout the domain for the temperatures and velocities in the two phases. In the VOF model, energy (E) and temperature (T) are treated as mass-averaged variables:

$$E = \frac{\sum_{q=1}^{n} \alpha_q \rho_q E_q}{\sum_{q=1}^{n} \alpha_q \rho_q}, \tag{7}$$

where E_q is based on the specific heat of the q^{th} phase and the shared temperature.

Evaporation and condensation at the interface are modeled as a source term in the continuity equation for the volume fraction (Eq. 4), i.e.:

$$S_{\alpha_q} = \dot{\mathbf{m}}_i \cdot \mathbf{A}_i\,, \tag{8}$$

where $\mathbf{A}_i$ is an interfacial area density vector, and $\dot{\mathbf{m}}_i$ is a mass flux vector, which for near equilibrium conditions can be determined based on the Schrage[7] equation:

$$|\dot{\mathbf{m}}| = \left(\frac{2\sigma}{2-\sigma}\right)\left(\frac{M}{2\pi R}\right)^{1/2}\left(\frac{P_i}{T_i^{1/2}} - \frac{P_v}{T_v^{1/2}}\right). \tag{9}$$

Here σ is the accommodation coefficient (value of 0.001 was used in most cases in this study); M is the molar mass of the fluid; R is the universal gas constant; P_i and P_v are, respectively, the interfacial and vapor pressures (it was assumed that $P_i \cong P_{sat}$); T_i and T_v are, respectively, the interfacial and vapor temperatures (it was assumed that $T_i = T_v \cong T_{sat}$ at the interface). Finally, $\mathbf{A_i}$ is defined as:

$$\mathbf{A}_i = |\nabla \alpha|, \tag{10}$$

where α is the volume fraction of the primary phase.

In the present implementation, the surface tension forces at the interface are modeled via the Continuum Surface Force (CSF) model of Brackbill et al.[8]. In this model, the surface tension forces at the interface are transformed into a volume force ($\mathbf{F}_{vol}$), which is added as a source to the momentum equation:

$$\mathbf{F}_{vol} = \sum_{pairs\ ij, i<j} \sigma_{ij} \frac{\alpha_i \rho_i h_i \nabla \alpha_j + \alpha_j \rho_j h_j \nabla \alpha_i}{\frac{1}{2}(\rho_i + \rho_j)}\,, \tag{11}$$

where h_i is the surface curvature calculated from the local gradients in the surface normal at the interface:

$$h_i = \nabla \cdot \hat{\mathbf{n}}. \tag{12}$$

C. Turbulence Modeling

In this study, three different turbulence models are used with the VOF model and compared against each other and experimental data. The first two are the Shear Stress Transport k-ω model of Menter[9] (kw-SST) used with and without Turbulence Damping (TD) at the interface. And the third model is the Improved Delayed Detached Eddy Simulation (IDDES) model proposed by Shur et al.,[10] and Gritskevich et al.[11]. A Laminar simulation (without any

turbulence modeling) was also performed, and its results are compared with the results of simulations with turbulence models.

Shear Stress Transport k-ω model of Menter[9] (kw-SST) is similar to the standard k-ω model of Wilcox,[12] but has the ability to account for the transport of the principal shear stress in adverse pressure gradient boundary layers. These features make the kw-SST model more accurate and reliable for a wider class of flows than the standard k-ω model.

In multiphase flows, a high velocity gradient at the interface between two fluids results in high turbulence generation, in both phases. Hence, Turbulence Damping (TD) can be used in the interfacial area to model such flows correctly. For the kw-SST model, the following source term is added to the ω-equation[13]:

$$S_i = A_i \Delta n \beta \rho_i \left(\frac{B6\mu_i}{\beta \rho_i \Delta n^2} \right)^2, \tag{13}$$

where

A_i = Interfacial area density for phase i
Δn = Cell height normal to interface
β = k-ω model closure coefficient of destruction term, which is equal to 0.075
B = Damping factor (a value of 100 was used in this study)
μ_i = Viscosity of phase i
ρ_i = Density of phase i

The Improved Delayed Detached Eddy Simulation (IDDES) model[10,11] is a hybrid RANS-LES model that provides a more flexible and convenient scale-resolving simulation (SRS) model for high Reynolds number flows. IDDES uses RANS in the boundary layer and LES in the detached regions, or bulk flow. This allows to resolve turbulent features in the detached regions with a benefit of not applying LES in the boundary layer which would be impractical for most applications. See model's details in the original publications of Shur et al.,[10] and Gritskevich et al.[11].

In the VOF model, continuity of the turbulent quantities is inherently assumed since one set of equations for the turbulent kinetic energy and dissipation rate is solved for both phases throughout the domain, with properties varying according to the local volume fraction value.

V. Numerical Implementation

A flightweight hydrogen storage tank, also known as K-Site, was considered for model validation. The tank is an ellipsoidal volume of revolution with major diameter of 2.2 m and major-to-minor axis ratio equal to 1.2. Tank geometry and computational mesh are shown in Figure 1a. The tank wall has a variable thickness with most of the wall being 2.08 mm thick except for the bolted flange and lid at the top, lands for support lugs, and thickened equatorial region. Liquid Hydrogen and its vapor fill the tank at a 49% liquid fill level. Heat fluxes, uniformly distributed along tank wall, of 2 and 3.5 W/m^2 are considered. The effect of modeling conjugate heat transfer between the fluid and solid tank wall, as well as an effect of wall thickness/geometry are discussed in the paper.

D. Initial Conditions

In this case measured initial ullage and tank wall temperature profiles reported by Hasan et al.[1] are applied. Initial liquid fill level is set to 49% by volume. In the cases where turbulence models are used initial values for turbulence kinetic energy and specific dissipation rate are set, respectively, to 1e-06, m^2 /s^2 and 100, 1/s.

E. Boundary Conditions

The tank wall, made of 2219 aluminum, is included in calculations in most cases. Two different tank wall thicknesses are considered: uniform "thin" wall (2.08 mm), and a variable tank wall (as shown in Fig. 1.). A simulation was also performed without tank wall. In the cases without the tank wall included in calculations heat flux is applied uniformly at the inner tank wall location. In the cases with conjugate heat transfer a uniform heat flux is applied at the outer tank wall location and coupled heat transfer is modeled at the inner tank wall location. A contact angle between liquid and the tank wall is assumed to be 0 degrees. No slip boundary conditions are applied on the inside of the tank wall which is in contact with fluid. Uniform heat fluxes of 2 or 3.5 W/m^2 are applied at the outside wall boundary to match experimental conditions.

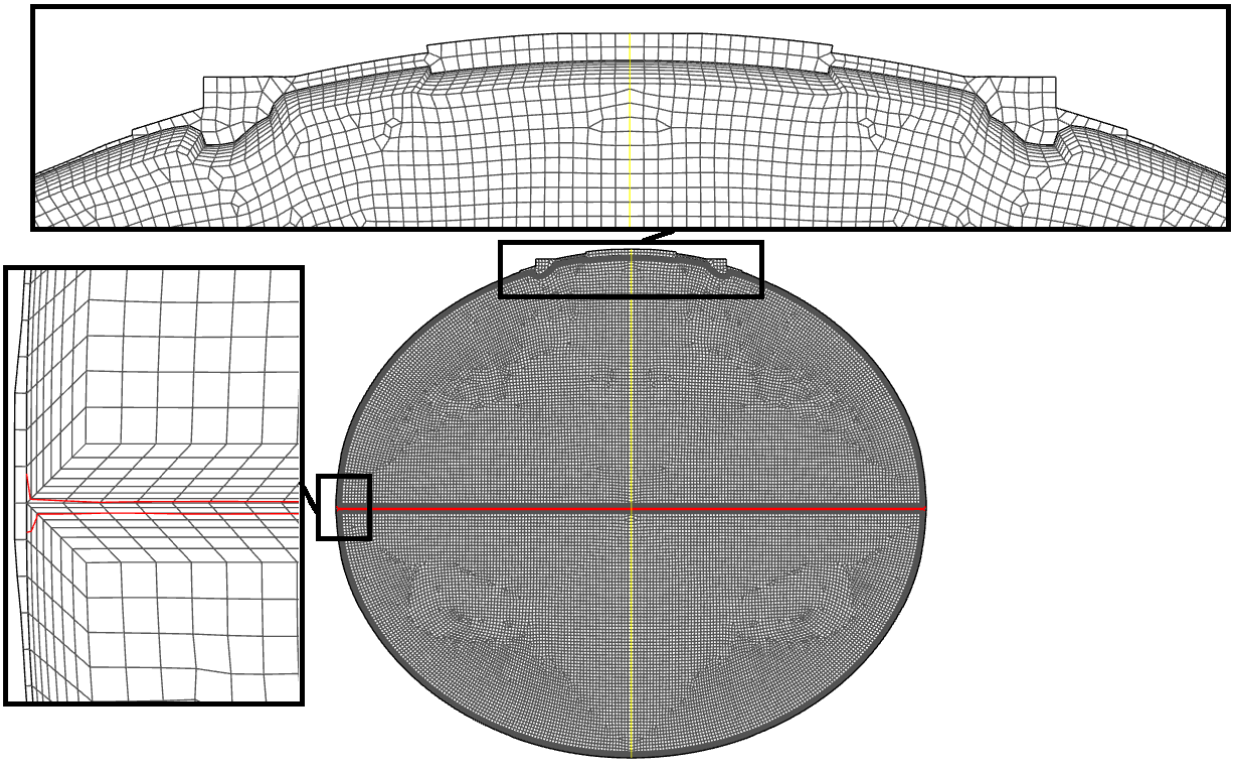

Figure 1a: Tank geometry and computational mesh

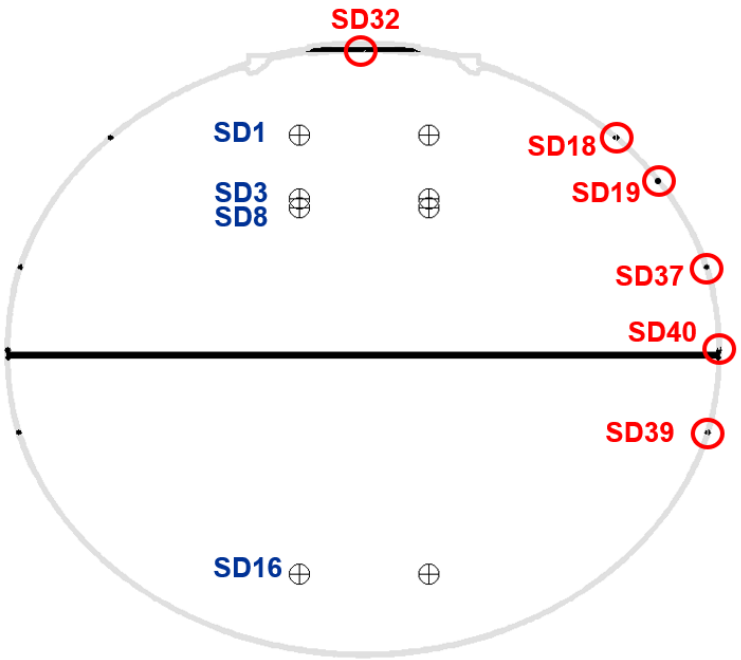

Figure 1b: A schematic of the tank with fluid and wall temperature probe locations used for comparison in this study.

F. Material Properties

The liquid hydrogen and its vapor fill the tank. Parahydrogen properties from NIST REFPROP database are used. Constant properties at saturation at the initial tank pressure are applied, except for thermal conductivity, viscosity, and specific heat, which are temperature dependent.

The tank wall material is modeled with constant density and temperature dependent properties for thermal conductivity and specific heat.

G. Discretization and Convergence

The Second Order Upwind scheme is used to discretize the turbulence, energy, and momentum equations (cell values). The PISO scheme is used for the pressure-velocity coupling (cell values). The Least Squares Cell Based scheme is used for the gradient calculations (face values). The Body Force Weighted scheme is used for the pressure interpolation (face values). The Point Implicit (Gauss-Seidel) linear equation solver with the Algebraic Multi-Grid (AMG) method is used to solve the linearized systems of equations. The Bounded Second Order Implicit temporal discretization and the Compressive scheme for the VOF equation is used with the implicit VOF model. The convergence criteria are set to $1x10^{-4}$ for all the equations except the energy equation, for which it is set to $1x10^{-6}$. Time step size value of 0.05 seconds is used in most cases.

H. Computational Mesh

2D axisymmetric computational grid used in most cases in the current study is shown in Fig. 1a. The mesh is refined near the tank walls and near the liquid-vapor interface to resolve interfacial heat and mass transfer. The grid size used in this study is ~15,000 cells.

VI. Results and Discussion

CFD simulations results are presented and compared with the data obtained in the experiment[1] in this section. The results of the cases with the heat flux value equal to 3.5 W/m^2 are presented first, followed by the results of the cases with the heat flux value equal to 2 W/m^2.

I. 3.5 W/m^2 Heat Flux

1. The Grid Independence Study

Three different computational meshes, shown in Fig. 2, are used in the grid independence study. This study was conducted with the IDDES turbulence model. These meshes have different refinements both near the liquid-vapor interface and near the tank wall, as well as different element sizes away from the walls or interface. Characteristics of computational meshes used in the grid independence study are summarized in Table 1. Different levels of refinement are reflected in the total number of elements for each grid, as depicted in Table 1. Effect of the grid size on the tank pressure during pressurization is presented in Fig. 3. Both medium and fine meshes result in similar tank pressures when the coarse mesh under-predicts the tank pressure. The medium grid was selected for the rest of the studies presented in this paper. The grid independence study is conducted using tank geometry with uniform "thin" (2.08 mm) tank wall. Cases with variable wall thickness presented here have mesh characteristics similar to the ones of the medium mesh.

Table 1. Characteristics of computational meshes used in the grid independence study.

	Cell size near the wall, $x10^{-3}$ m	Cell size near the interface, $x10^{-3}$ m	Element size away from the wall and interface, $x10^{-3}$ m	Total number of elements
Coarse mesh	3	3	14	10,517
Medium mesh	1.5	1.5	12	25,269
Fine mesh	0.5	0.5	8	43,671

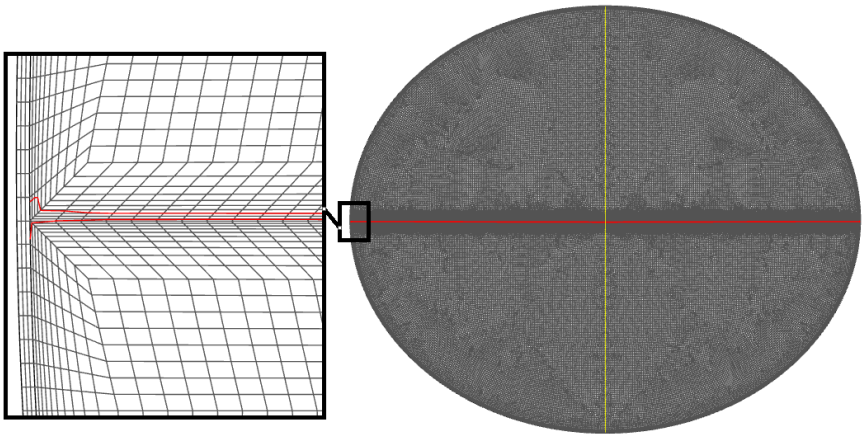

a)

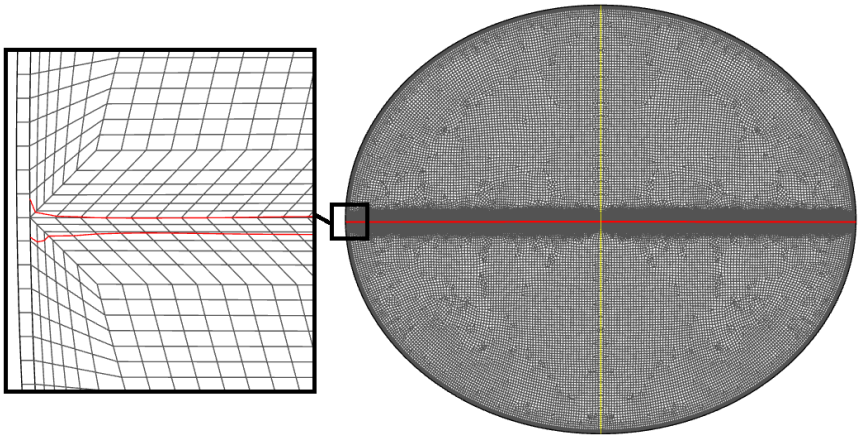

b)

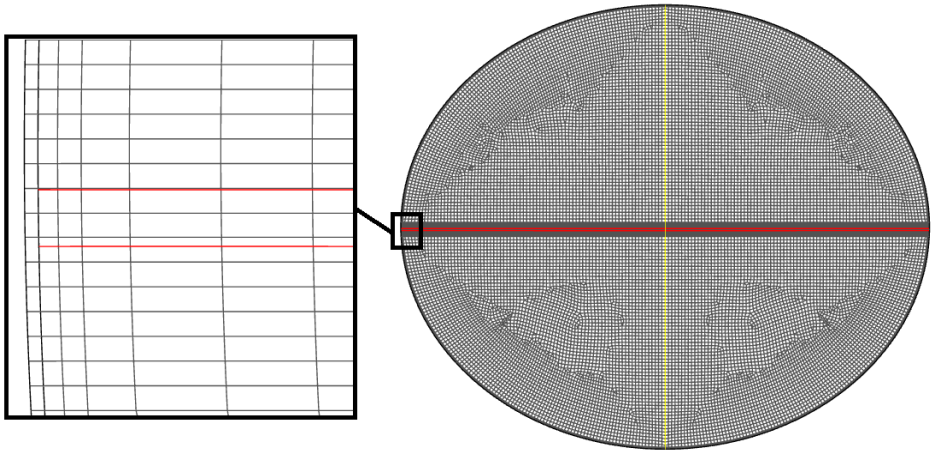

c)

Figure 2: Computational meshes used in the grid independence study (a-fine mesh (44,000 cells), b-medium mesh (25,000 cells), c-coarse mesh (11,000 cells))

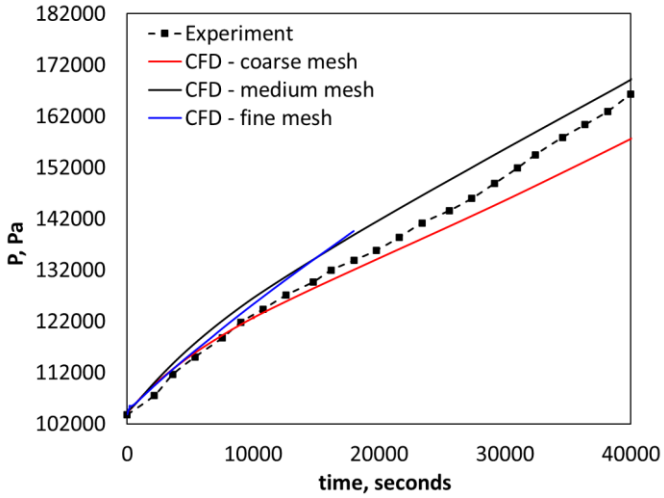

Figure 3: Results of the grid independence study

2. The effect of the accommodation coefficient

Three different values of the Accommodation Coefficient (AC) (see Eq. 9) equal to 0.01, 0.001 and 0.0001 were considered in order to study its effect on the predicted tank pressure and phase change rate during tank self-pressurization. The results, presented in Fig. 4, indicate that varying the value of AC between 0.001 and 0.0001 doesn't have any effect on the predicted tank pressure and that both values result in very similar predicted phase change rates. The highest value of AC = 0.01 results in a similar tank pressure, compared to the results of the other two AC values tested. However, increasing AC causes large oscillations in predicted values of the phase change rate. Also, in the case with the highest value of AC tested the time step size had to be reduced to 0.001 s, compared to cases with lower values of AC, where a time step size of 0.05 s was used to achieve convergence. This result is consistent with our previous finding regarding the effect of accommodation coefficient on interfacial mass transfer under near equilibrium conditions for both VOF-captured and Sharp Interface models[14].

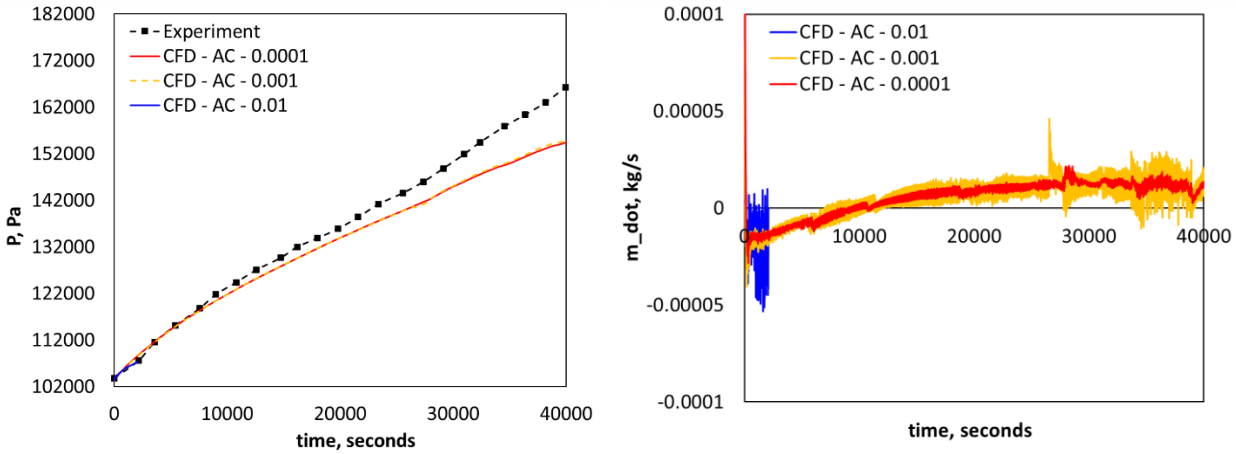

a) tank pressure **b) phase change rate**

Figure 4: The effect of accommodation coefficient on predicted tank pressure (a) and phase change rate (b)

3. The effect of the tank wall geometry

The effect of the tank geometry on the tank pressure and temperatures was studied and the results are presented in this section. Tank pressures, vapor temperatures and phase change rates predicted by the models with a uniform "thin" wall (2.08 mm), variable tank wall and without tank wall are presented and compared with the experimental data in Fig. 5. As shown in the figure, the variable thickness tank wall model predicts a lower tank pressure in

comparison to the models with the uniform "thin" wall and without the tank wall. However, including variable tank wall geometry into the model improves noticeably the vapor temperature predictions at the top (SD1) and in the middle of the vapor region (SD8) as shown in Fig. 5b. The vapor temperatures are significantly over-predicted in the case without tank wall. This suggests that accounting for conjugate heat transfer is essential for accurate predictions of tank pressure and temperatures during self-pressurization. Evolutions of the phase change rate at the liquid-vapor interface predicted by the tree models are shown in Fig. 5c. Here the models with the tank wall predict vapor condensation during first 10,000 seconds of self-pressurization followed by evaporation (positive values of the phase change rate) afterwards. The case without the tank wall predicts larger amounts of condensation and no transition into evaporation.

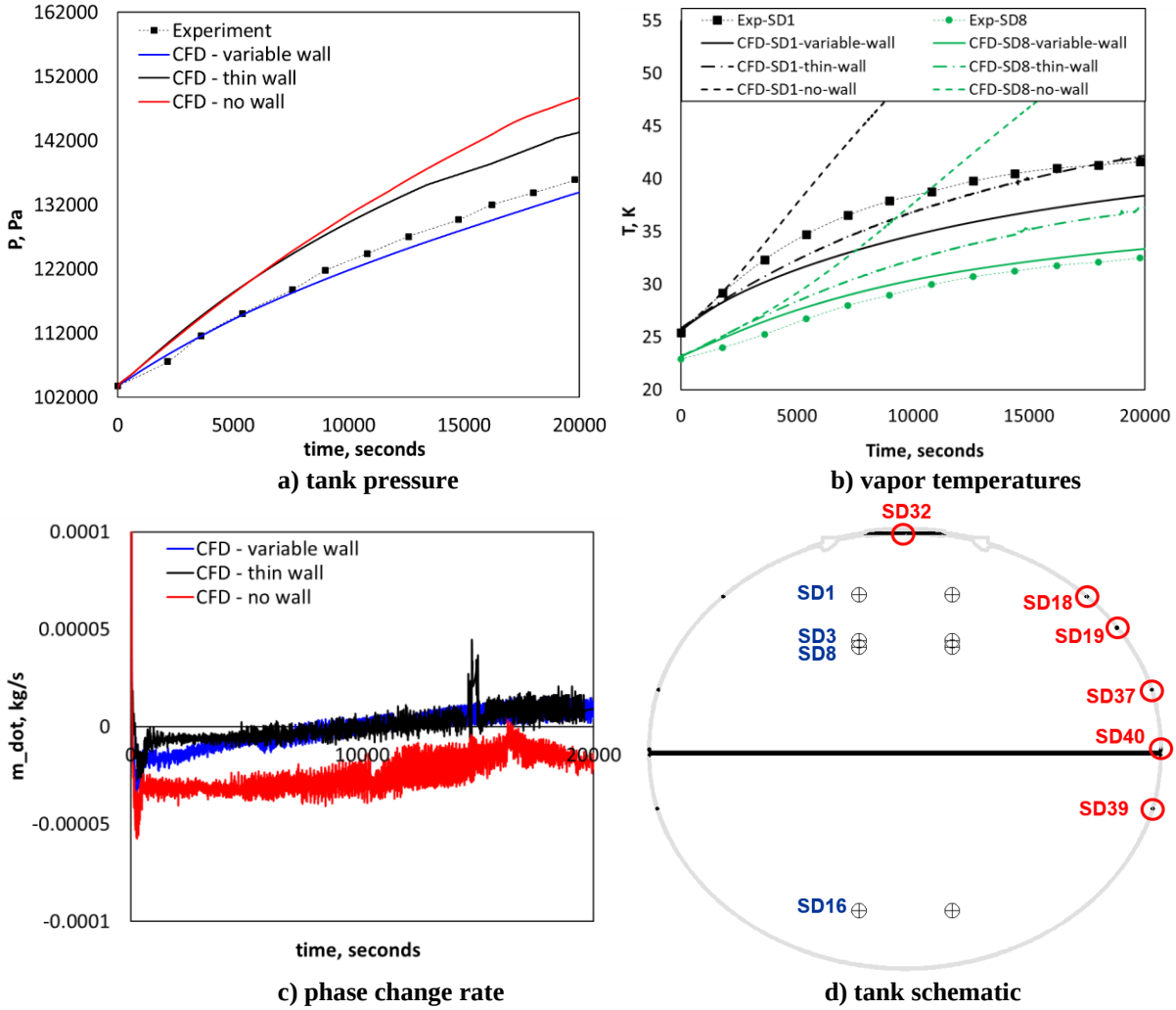

Figure 5: The effect of modeling tank wall thickness/geometry on tank pressure (a), vapor temperatures (b), and phase change rate (c)

4. The effect of turbulence modeling

The effect of turbulence modeling was studied, and results are reported in this section. Three different turbulence models are considered. These models are the two-equations kw-SST with and without turbulence damping at interface, and the scale-resolving Improved Delayed Detached Eddy Simulation (IDDES) model. A laminar simulation, where no turbulence models are used, was performed as well, even though the natural convection flow is turbulent in this case (vapor: Gr = 2.21e+13; liquid: Gr = 1.33e+14). A more detailed explanation for this apparent fidelity of the laminar model for seemingly turbulent natural convective situations can be found in our previous paper[14]. The effects of turbulence modeling on the tank pressure and interfacial phase change rate are presented in Figures 6a and 6b

respectively. As shown in Fig. 6a, the laminar model predicts tank pressures during self-pressurization which are very close to the values measured in the experiment.

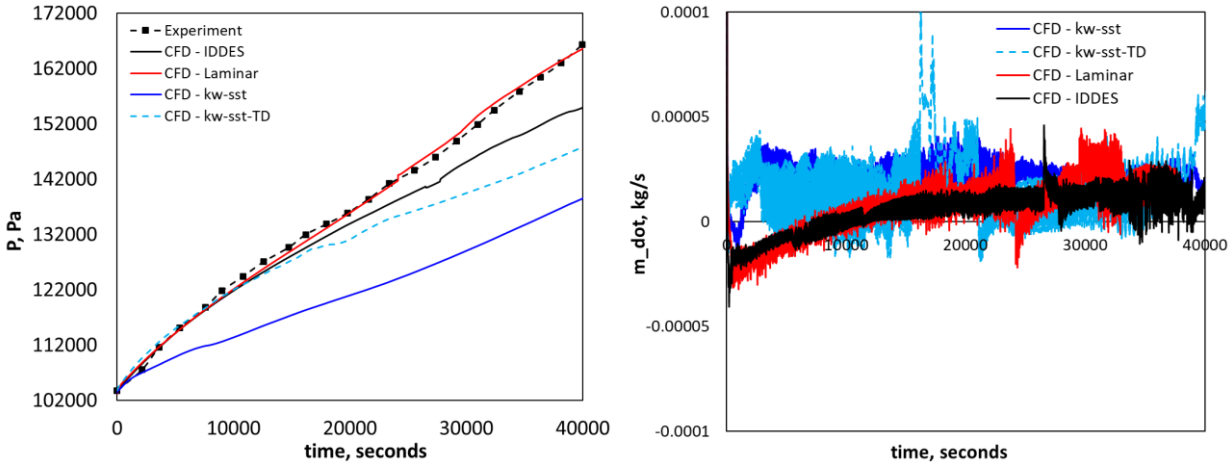

a) tank pressure **b) phase change rate**

Figure 6: The effect of turbulence modeling on tank pressure (a) and phase change rate (b)

The kw-SST model without turbulence damping significantly under predicts tank pressure compared to the experimental data and the laminar model results. The kw-SST model with turbulence damping shows improvements in the tank pressure predictions, especially, for the first 15,000 seconds, however, it significantly under predicts tank pressure for the rest of the simulation. The IDDES model shows a significant improvement in tank pressure predictions compared to the kw-SST simulations with and without turbulence damping. However it still under predicts experimental pressure at the end of self-pressurization. The laminar and IDDES models predict similar values of the phase change rate throughout the simulation. Both models predict condensation during the first 10,000 seconds of the tank self-pressurization and evaporation for the rest of the simulation. The kw-SST models with and without turbulence damping predict larger amounts of evaporation in the beginning of the simulation with an averaged interfacial evaporation rate that matches the results of the laminar and IDDES models after 20,000 seconds.

Fluid temperatures at different measurement locations predicted by three different turbulent and a laminar model are compared with each other and with the experimental data in Figure 7.

A schematic of the tank with temperature measurement locations is shown in Figure 7b for reference. The laminar and IDDES models predict vapor temperatures at the top and middle of the vapor region reasonably well compared to the experimental data as shown in Figures 7a and 7c. The kw-SST models with and without damping significantly under predict vapor temperatures compared to the experiment and results of the laminar and IDDES models. Predicted liquid temperatures near the bottom of the liquid region are presented and compared with the experimental data in Figure 7d. As shown in this figure, the results of the kw-SST turbulence model without turbulence damping provide the best agreement with the experimental data at this measurement location. The laminar model under predicts liquid temperatures. The IDDES model shows an improvement over the laminar model at predicting liquid temperatures that are very close to the predictions of the kw-SST with turbulence damping model. Predicted tank wall temperatures are compared between the IDDES and the laminar CFD models and experimental data in Figure 8. Both CFD models predict very similar wall temperatures at all locations which are in a reasonably good agreement with the experimental data for the wetted wall and up to the middle of the dry wall on the vapor side. At the two measurement locations at the top of the vapor region, CFD models under predict measured temperatures. This could be due to heat leaks through the top lid of the tank, where various tank instrumentation passes through. These leaks are not included in the CFD model.

Temperature contours and streamlines in the tank at the end of self-pressurization are presented in Figure 9. A comparison between the laminar, IDDES and kw-SST with turbulence damping models is shown. As can be seen in the figure, both laminar and IDDES models predict considerable stratification in the vapor, but the kw-SST model with turbulence damping predicts a well-mixed vapor with temperatures significantly lower than the ones predicted by the other two models. Streamlines predicted by the kw-SST model also indicate significant mixing in the vapor region while the streamlines predicted by the other two models do not.

Contours of turbulent kinetic energy predicted by the IDDES, and kw-SST turbulence models are presented in Figure 10. Tank geometry with a "thin" tank wall is used in this comparison. The kw-SST turbulence model predicts elevated turbulence levels in the vapor region while the IDDES model shows lower levels of turbulence in the vapor. This is consistent with the findings of the well-mixed vapor region predicted by the kw-SST model. Turbulence damping used with the kw-SST model does not affect the predicted turbulence levels in the vapor because damping is only applied at the interface. The IDDES turbulence model does not seemingly over-predict turbulence and mixing in the vapor which results in improved predictions of the tank pressure and vapor temperatures.

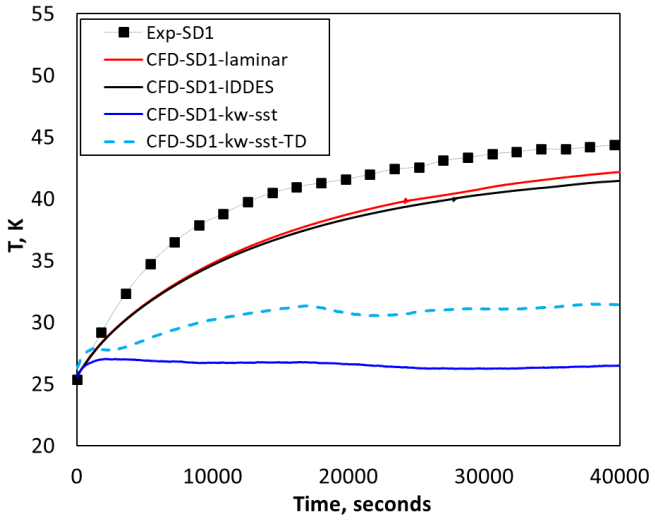

a) SD1 - vapor

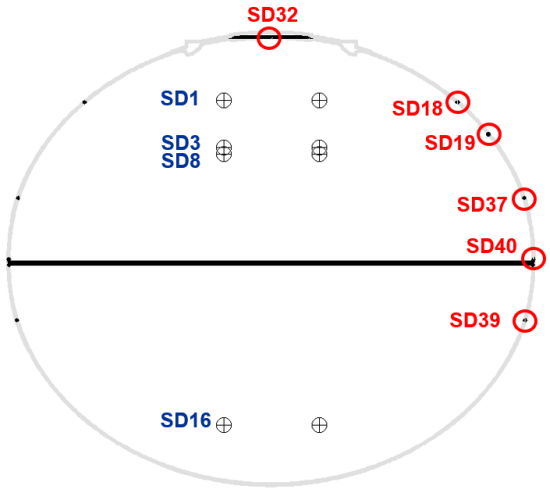

b) tank schematic

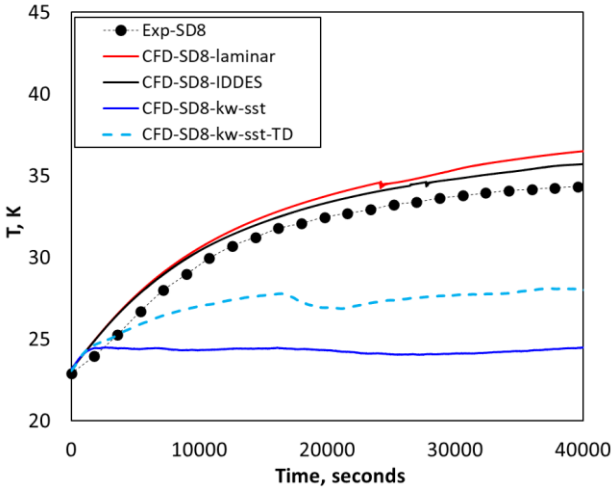

c) SD8 - vapor

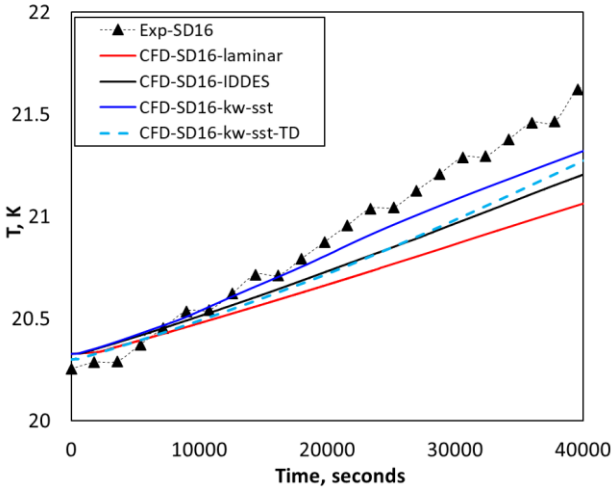

d) SD16 - liquid

Figure 7: The effect of turbulence modeling on predicted fluid temperatures at SD1 (a) and SD8 (c) measurement locations in the vapor and SD16 (d) measurement location in the liquid.

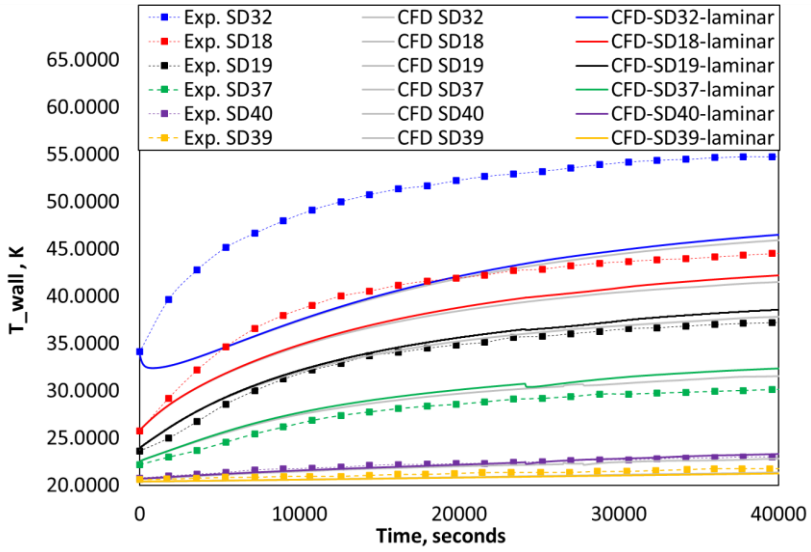

Figure 8: The effect of turbulence modeling on tank wall temperatures

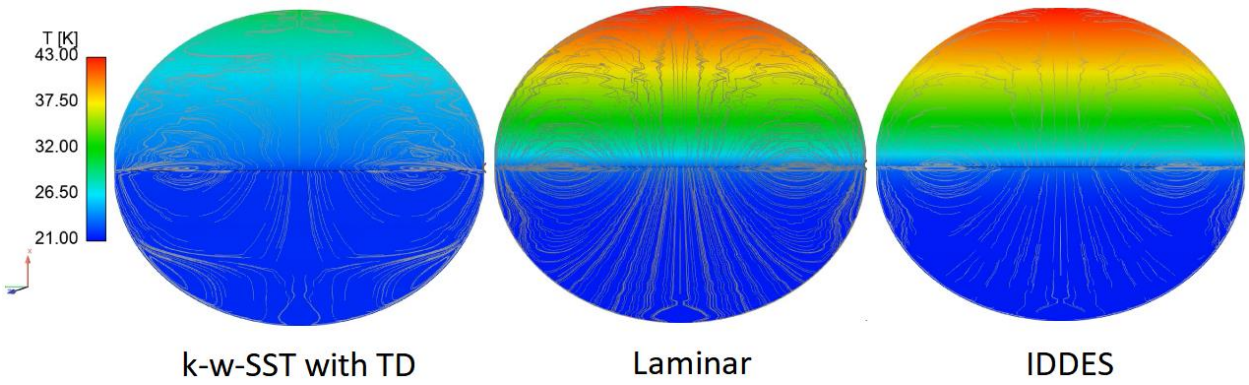

Figure 9: The effect of turbulence modeling: temperature contours and streamlines

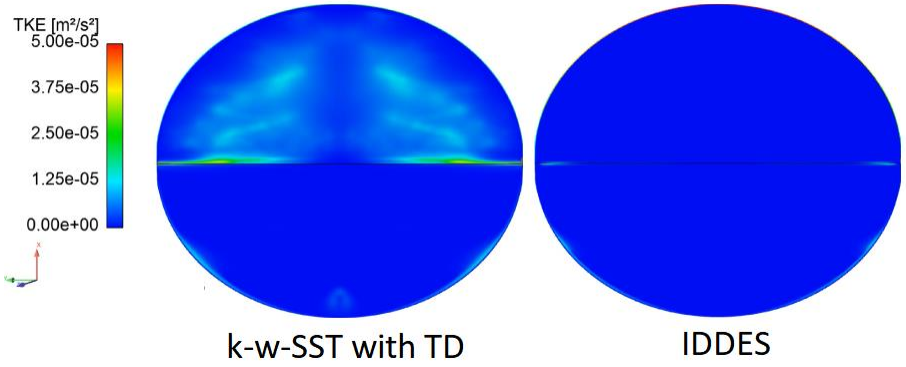

Figure 10: The effect of turbulence modeling: Turbulent Kinetic Energy contours

This is further illustrated by comparing effective (a sum of molecular and turbulent) thermal conductivities predicted by the IDDES and kw-SST with turbulence damping models in Figure 11. There the IDDES model shows significantly lower values in both liquid and vapor regions, compared to the results of the kw-SST model with turbulence damping at the interface. However, in the diffused interface region both models predict lower values of the

effective thermal conductivity on both sides of the interface (at vapor volume fraction value of 0.1 representing the liquid side and vapor volume fraction value of 0.9 representing the vapor side) as shown in Figure 12. The values of the effective thermal conductivity calculated by both models in the interfacial region are close to the molecular values (represented by red lines in Fig. 12) for both liquid and vapor.

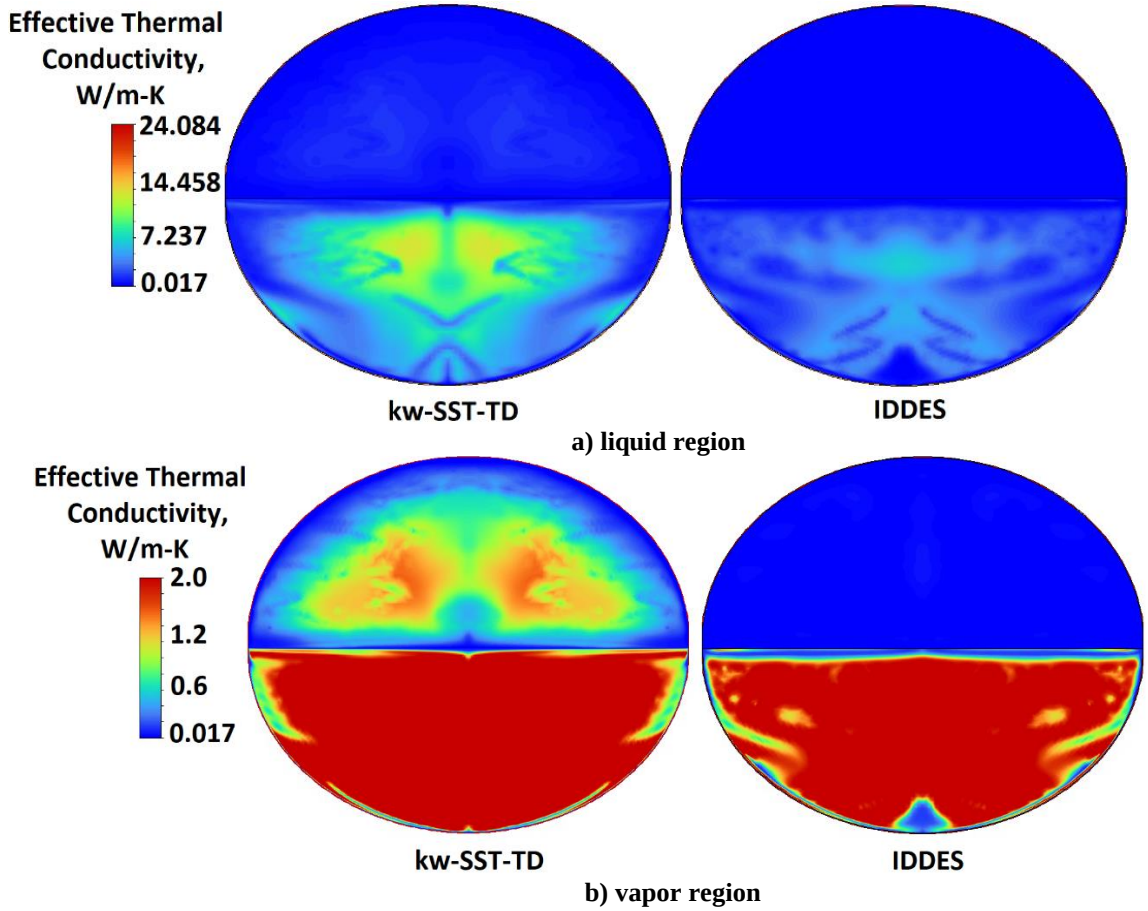

Figure 11: The effect of turbulence modeling: Effective Thermal Conductivity contours (full range – a; reduced range to represent the vapor region – b)

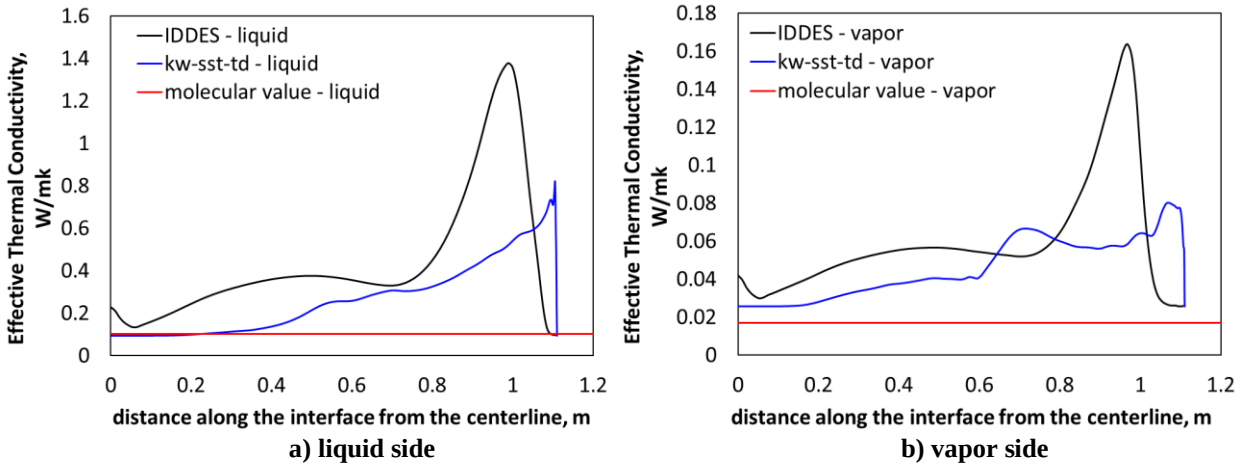

Figure 12: The effect of turbulence modeling on the Effective Thermal Conductivities at the liquid side (a) and vapor side (b) of the interface

J. 2 W/m^2 Heat Flux

Predicted tank pressures during tank self-pressurization with the heat flux value equal to 2 W/m^2 are presented and compared with the experimental data in Figure 13. Here, just like in the case with the 3.5 W/m^2 heat flux value, the laminar model predictions are closer to the measured values (within 3%), compared to the results of the turbulent (k-w-SST) model, which under predict the measured tank pressure during pressurization (by 16%). In this case the IDDES model also shows an improvement over the kw-SST model, predicting tank pressure within 5% of the experimental values.

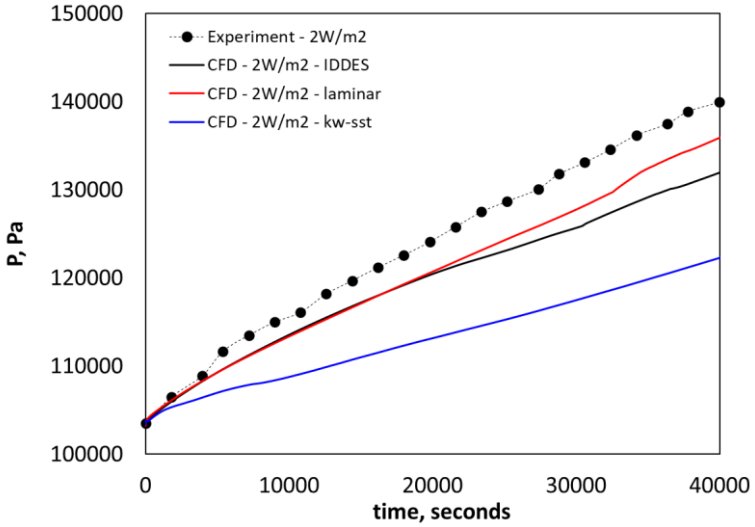

Figure 13: Tank pressure during tank pressurization with 2 W/m^2: CFD vs. Experiment

VII. Conclusion

A CFD model of a cryogenic tank self-pressurization was developed and validated against 1g experimental data provided by Hasan et al.[1]. Simulations with 2 and 3.5 W/m^2 wall heat fluxes were performed. Predicted tank pressure and fluid and wall temperature evolutions are compared with the experiemntal data. The results of three different turbulence models are compared with the results of the laminar model and with the experimental data. The effects of the tank wall geometry and Accommodation Coefficient (AC), used for predicting phase change rate at the interface, are evaluated.

The laminar VOF with conjugate heat transfer model compares well with the measured tank pressure values. Predicted tank pressures are within 1% of the measured ones for the 3.5 W/m^2 heat flux case and within 3.5% for the 2 W/m^2 heat flux case. Three different turbulence models were evaluated in this study. The traditional RANS kw-SST turbulent VOF model with conjugate heat transfer performs poorly, predicting tank pressure during self-pressurization within 15% of the measured values. Introduction of turbulence damping at the interface with the kw-SST model improves model's pressure predictions, but only slightly from 15% to 12% of the measured values. However, utilizing a scale-resolving RANS-LES blended IDDES turbulence model results in an improvement of the tank pressure prediction from 15% to 7% of the measured values. It is worth mentioning that, for the studied type of flow and heat transfer, the IDDES model requires similar computational resources as the RANS models, since it can be utilized with 2D axisymmetric meshes. On the other hand, an LES model requires a fine 3D mesh that will be drastically more computationally expensive. Significant improvements in predicting tank fluid temperatures are observed with the IDDES model as well. Vapor temperatures are predicted within 4-6.5% of the measured values by the IDDES model and under-predicted by up to 40% by the kw-SST model. The kw-SST turbulence model predicts enhanced mixing and elevated levels of turbulence in the vapor region, compared to the results of the IDDES model. This results in under-predicting vapor temperatures and tank pressure. Despite significantly better performance of the IDDES model over the traditional RANS models, the laminar model still predicts tank pressure better during the self-pressurization process. There is a need to further investigate the reason why laminar VOF model is in a better agreement with experimental pressure values, even though the natural convection flow inside the tank is turbulent (vapor: Gr = 2.21e+13; liquid: Gr = 1.33e+14).

The tank wall geometry in the CFD model significantly affects predicted tank pressure and temperatures. A uniform "thin" wall (uniform wall thickness of 2.08 mm) results in higher tank pressures and vapor temperatures, compared to a more realistic variable tank wall geometry case, where predicted vapor temperatures are in a better agreement with the experimental data.

The value of AC has little effect on the tank pressure and interfacial phase change rate predictions. However, increasing the value of AC above 0.001 in this study resulted in large interfacial mass transfer oscillations and required significantly (an order of magnitude) lower time step sizes.

The results of this investigation effort showed that our customized storage tank CFD model implemented in ANSYS Fluent CFD code can predict tank pressures during self-pressurization of a large tank in normal gravity within 3% of the measured values with the laminar model and 7% with the scale resolving IDDES turbulence model.

Acknowledgments

Authors would like to thank the Modeling Portfolio Project within the STMD CFM Project Office for providing funding for this work.

References

[1] Hasan, M. M., Lin, C. S., Van Dresar, N. T., "Self-Pressurization of a Flightweight Liquid Hydrogen Storage Tank Subjected to Low Heat Flux," NASA TM-103804, 1991

[2] Lan, E., Shi, S., Ji, W., Ishii, M. "Modeling and simulation of cryogenic propellant tank pressurization in normal gravity", Applied Thermal Engineering, Vol. 236, Part D, 2024.

[3] M. Kassemi, S. Hylton, O. Kartuzova, "1G and Microgravity Tank Self-Pressurization: Experiments and CFD Model Validations across Ra and Bo Regimes", International Journal of Microgravity Science and Application, Vol 37, No.1, 2020, p. 370103-1.

[4] O. Kartuzova, M. Kassemi, J. Agui and J. Moder "Self-Pressurization and Spray Cooling Simulations of the Multipurpose Hydrogen Test Bed (MHTB) Ground Based Experiment" 50th AIAA/ASME/SAE/ASEE Joint Propulsion Conference proceedings, July 2014, Cleveland, OH, AIAA2014-3578

[5] R. J. Stochl, and R. H. Knoll "Thermal performance of a liquid hydrogen tank multilayer insulation system at warm boundary temperatures of 630, 530, and 152 R" 27th AIAA/ASME/SAE/ASEE Joint Propulsion Conference proceedings, June 1991, Sacramento, CA

[6] C.W. Hirt and B.D. Nichols, "Volume of fluid (VOF) method for the dynamics of free boundaries", Journal of Computational Physics **39** (1): 201-225. 1981.

[7] R.W. Schrage, A theoretical study of interphase mass transfer, Columbia University Press, New York, 1953.

[8] Brackbill J.U., Kothe, D.B., Zemach, C., "A continuum method for modeling surface tension," J. Comp. Phys. Vol. 100, 1992, pp. 335–354.

[9] Menter, F. R., "Two-Equation Eddy-Viscosity Turbulence Models for Engineering Applications," AIAA Journal, 32(8), 1994, pp. 1598-1605.

[10] M. L. Shur, P. R. Spalart, M. K. Strelets, and A. K. Travin. "A Hybrid RANS-LES Approach with Delayed-DES and Wall-Modelled LES Capabilities". International Journal of Heat and Fluid Flow. 29:6. December 2008. 1638-1649.

[11] M. S. Gritskevich, A. V. Garbaruk, J. Schutze, F. R. Menter. "Development of DDES and IDDES Formulations for the k-ω Shear Stress Transport Model". Flow, Turbulence and Combustion. 88(3). 431–449. 2012.

[12] Wilcox, D.C., *Turbulent Modeling for CFD*, DCW Industries, Inc., La Canada, California, 1998.

[13] Y. Egorov. "Contact Condensation in Stratified Steam-Water Flow". EVOL-ECORDA-D 07. 2004.

[14] M. Kassemi and O. Kartuzova, Effect of Interfacial Turbulence and Accommodation Coefficient on CFD Predictions of Pressurization and Pressure Control in Cryogenic Storage Tank, Cryogenics, Vol. 74, pp.138-153, 2016.